Moist Dynamics and Orographic Precipitation in Northern and Central California during the New Year's Flood of 1997

JOSEPH GALEWSKY AND ADAM SOBEL

Department of Applied Physics and Applied Mathematics, Columbia University, New York, New York

(Manuscript received 20 May 2004, in final form 29 November 2004)

ABSTRACT

The dynamics of moist orographic flows during the January 1997 floods in northern and central California are investigated using numerical simulations computed with the fifth-generation Pennsylvania State University–National Center for Atmospheric Research (PSU–NCAR) Mesoscale Model (MM5). Early in the event (31 December 1996–1 January 1997), the low-level winds offshore of California's central coast were blocked by the topography of the Santa Lucia Range, and the low-level winds in the Central Valley were blocked by the topography of the central Sierra Nevada Range. In contrast, moisture-laden winds along the northern Coast Ranges and the northern Sierra Nevada flowed over topographic barriers. As the core of humid air migrated to the south over 24 h, the low-level barrier jets weakened as the atmospheric stability decreased, bringing heavy rainfall to the central and southern Sierra Nevada at the end of the event. The heavy precipitation during this event was largely controlled by the interaction of the flow with topography, with little contribution from non–topographically forced dynamical uplift. Latent heating was essential for lowering the effective stability of the flow and allowing the winds to flow over mountainous terrain, particularly in the northern Coast Ranges, and for enhancing the low-level jet and associated moisture transport. The horizontal distribution of static stability played a key role in the event by setting up a complex combination of flow-over and flow-around regimes that enhanced uplift in the northern Sierra Nevada during the period of heaviest rainfall.

1. Introduction

a. Overview

The flooding that affected northern and central California (Fig. 1) during late December 1996 and the first week of January 1997 was among the worst on record for the state, causing at least $1.6 billion in property damage and damaging or destroying approximately 16 000 homes (Lott et al. 1997). Peak river flows were the largest on record at 106 gauging stations, and recurrence intervals for events of this magnitude were estimated to be greater than 100 yr at 32 stations, primarily in the central and northern Sierra Nevada, ranging from Tuolumne County in the south to Plumas County in the north (Hunrichs et al. 1998). The storm also caused numerous landslides and debris flows in mountainous regions of California (De La Fuente and Elder 1998) and produced sediment fluxes on the Eel River shelf near Eureka that were two orders of magnitude greater than any other event that winter (Ogston et al. 2000).

Orographic effects contribute strongly to the regional characteristics of precipitation and flooding in California (Pandey et al. 1999; Leung et al. 2003; Ralph et al. 2003), and the interactions of moist flows with orography are likely to have played an important role in localizing heavy rainfall (e.g., Jiang 2003; Rotunno and Ferretti 2001). In this paper, we use numerical simulations to investigate the dynamics of the January 1997 floods in northern and central California. We are especially interested in understanding the processes that were responsible for the spatial and temporal distribution of heavy rainfall during this event because of their impact on surface hydrological processes such as streamflow and landsliding.

Corresponding author address: Joseph Galewsky, Department of Applied Physics and Applied Mathematics, Columbia University, New York, NY 10027.
E-mail: jg2282@columbia.edu

b. Theoretical background

Theories for the interaction of dry atmospheric flows with topography (Smith 1979; Chen and Smith 1987)

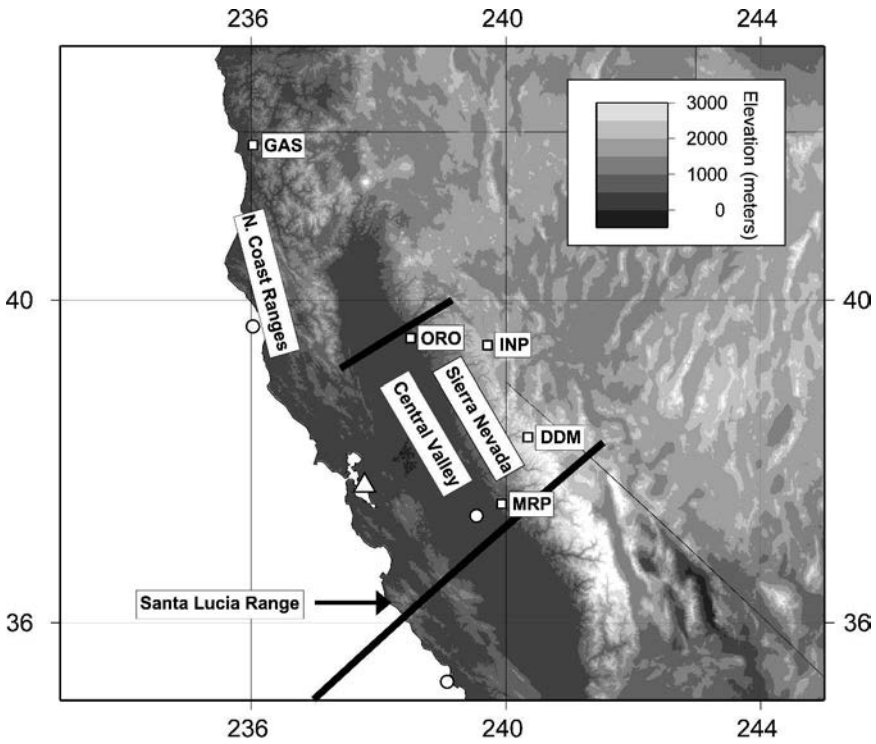

FIG. 1. Location map showing topography and geographic features mentioned in the text. The northern and southern heavy lines indicate locations of cross sections in Figs. 16 and 17, respectively. Circles indicate location of relative humidity time–height profiles in Fig. 18. Meteorological stations are indicated by squares: GAS—Gasquet Ranger Station (elevation 117 m); ORO—Oroville Dam (274 m); MRP—Mariposa Ranger Station (685 m); INP—Independence Lake (2109 m); DDM—Deadman Creek (2819 m). The Oakland rawinsonde site is indicated by a triangle.

show that the low-level flow tends to be blocked by mountainous topography when the Froude number

$$F_r = \frac{U}{h_m N} \tag{1}$$

is less than unity, where U is the cross-mountain wind speed, h_m is the mountain height, and N is the static stability $[(g/\theta_0)\partial\theta/\partial z]^{1/2}$, where θ_0 is constant mean potential temperature, and g is gravity. The effects of low-level blocking include upstream deceleration (Pierrehumbert 1984; Pierrehumbert and Wyman 1985; Smolarkiewicz and Rotunno 1990), downstream vortex shedding (Smolarkiewicz and Rotunno 1989), cold-air damming (Bell and Bosart 1988; Xiu 1990) and the development of barrier jets parallel to the topography (Overland and Bond 1993). Orographic blocking commonly occurs along the mountainous west coast of North America and can result in a complex mesoscale response in coastal regions (Doyle 1997; Steenburgh and Mass 1996) and along the Sierra Nevada (Parish 1982). The steepness of the mountain topography can be given by the Burger number (Overland and Bond 1993, 1995)

$$B = \left(\frac{h_m}{l_m}\right)\left(\frac{N}{f}\right), \tag{2}$$

where f is the Coriolis force, and l_m is the half-width of the ridge. For $B \ll 1$, the flow is quasigeostrophic and the flow proceeds over the topography. If $0.1 \leq B \leq 1.0$, the flow is semigeostrophic and depends only on B (Pierrehumbert and Wyman 1985). For $B > 1$ the mountainous topography can be considered hydrodynamically steep and the flow will be completely blocked. Numerical simulations (Pierrehumbert and Wyman 1985) indicate that the zone of deceleration will grow upstream to a width given by a Rossby radius of deformation

$$l_R = \frac{Nh_m}{f}. \tag{3}$$

The presence of moisture in the flow, however, adds substantial complexity to the dynamics just described. The latent heating that accompanies condensation acts to reduce the effective static stability of the flow (Dur-

ran and Klemp 1982) so that the effective moist F_r may be greater than unity, thereby favoring uplift and flow over the topography rather than blocking, even though the dry F_r may be less than unity. The problem for developing an analytic theory of moist orographic flow is that the boundary between saturated and unsaturated zones is generally not known a priori (Barcilon et al. 1979); therefore, much of the recent progress on this problem has come from idealized numerical simulations (e.g., Jiang 2003).

A further complexity is added when horizontal gradients of moisture are considered. In this case, the dynamics may favor either blocking or ascent, or complex combinations of the two regimes. Rotunno and Ferretti (2001) used idealized numerical simulations to show that the spatial and temporal distribution of precipitation in the 1994 Piedmont flood was dependent on a convergence between blocked and unblocked flows that was set up by a strong horizontal moisture gradient. As we describe below, the dynamics of the 1997 California floods depended on similar spatial variations of moisture and associated static stability.

c. Outline

This paper is organized as follows: First, the data used in the study are described. We then review the synoptic-scale meteorological conditions of the event. Next, we develop a control simulation (CTRL) that accurately reproduces the observed winds, precipitation, and temperature. We then introduce two numerical experiments, one without topography (NOTOPO) and another without latent heating (FDRY). The results of these simulations are then used to investigate some of the key physical processes controlling the event.

2. Data

The large-scale meteorological conditions for the event are illustrated by data from the National Centers for Environmental Prediction–National Center for Atmospheric Research (NCEP–NCAR) reanalysis dataset (2.5° latitude × 2.5° longitude resolution; Kalnay et al. 1996), selected rawinsonde profiles, and water vapor satellite imagery (Figs. 2–7). The initial and boundary conditions for the simulations presented here were derived from the 12-hourly NCEP Eta 40-km operational analysis. The model topography for the 30- and 10-km domains was derived from 10- and 5-min averaged U.S. Geological Survey (USGS) terrain data, respectively. Sea surface temperature and snow-cover data were obtained from the 2.5° NCEP Global Data Assimilation System (GDAS) analysis.

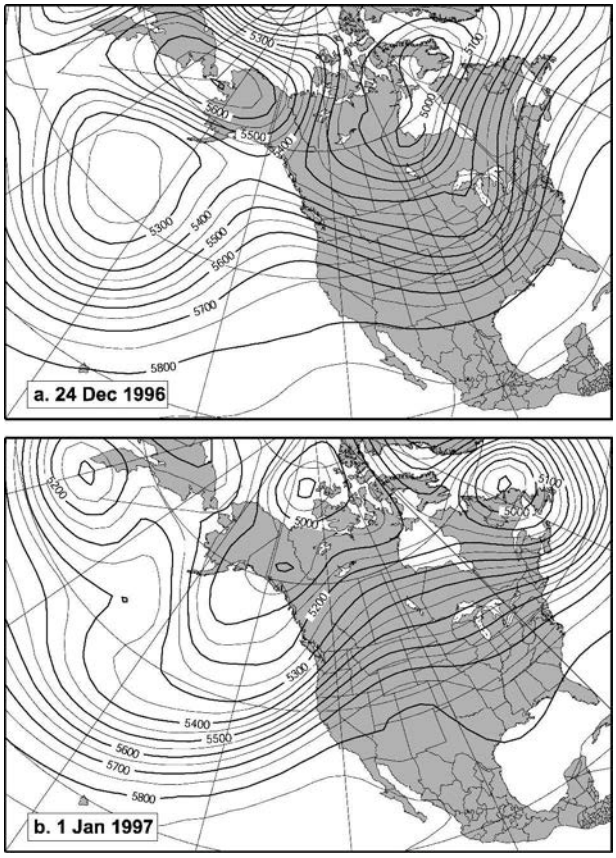

FIG. 2. NCEP–NCAR reanalysis of the 500-hPa height (m) on (a) 24 Dec 1996 and (b) 1 Jan 1997.

Precipitation data were derived from 224 rain gauges from a variety of sources, including the National Weather Service, the National Climatic Data Center (NCDC) cooperative observer program, and the California Department of Water Resources, and were gridded using a continuous curvature spline algorithm. Basic quality assurance (QA) steps included the removal of stations with data dropouts during the period, stations with unrealistic jumps in rainfall accumulation, and stations recording only trace amounts of rainfall when adjacent sites recorded significant rainfall. Even with QA, rain gauge data are potentially subject to significant errors and can underestimate rainfall by 5%–25% because of wind effects (Groisman and Legates 1994). Therefore, care should be exercised when comparing model estimates of precipitation to observations.

3. Case description

a. Climatological background

Recent studies have linked California wintertime floods to tropical intraseasonal variability (Higgins et

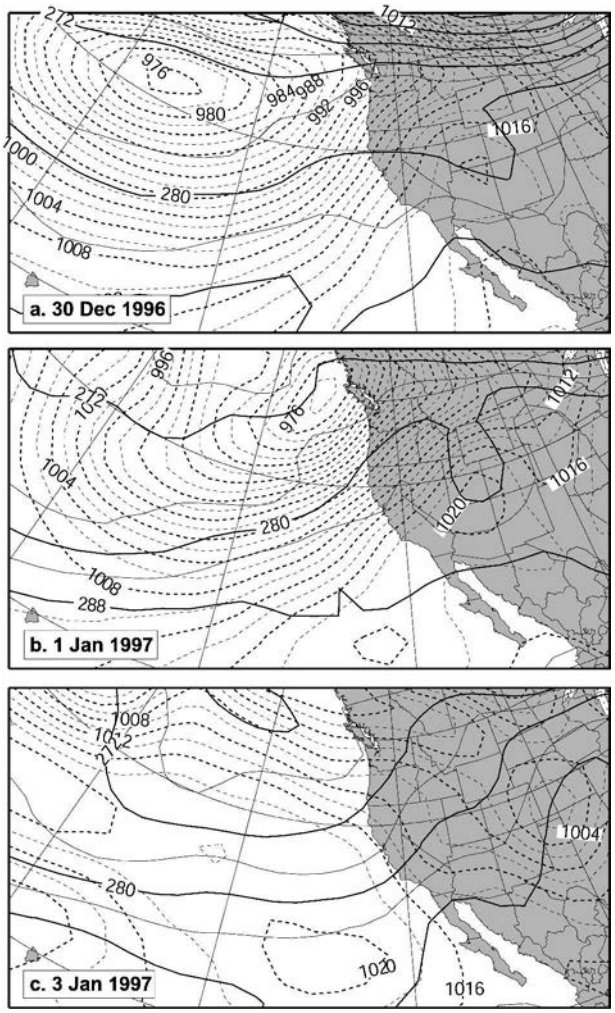

FIG. 3. NCEP–NCAR reanalysis of the sea level pressure field (hPa, dashed line) and 850-hPa temperature field (K, solid line) on (a) 30 Dec 1996, (b) 1 Jan 1997, and (c) 3 Jan 1997.

al. 2000). Statistically significant links have been established between the Madden–Julian oscillation (MJO) and extreme precipitation events in California, in which circulation anomalies over the eastern North Pacific enhance southwesterly flow into the West Coast (Mo and Higgins 1998b; Jones 2000). The moisture transport associated with these anomalies is often referred to as the Pineapple Express because much of the moisture flows over the Hawaiian Islands en route to the West Coast (Lackmann and Gyakum 1999). Higgins et al. (2000) found that the largest fraction of extreme precipitation events along the West Coast occur during ENSO-neutral years prior to the onset of El Niño. The California floods of January 1997 are an example of a Pineapple Express system and fit the pattern of Higgins et al. (2000) in that they occurred during an ENSO-neutral winter (1996/97) prior to a warm El Niño year (1997/98). The 15-day running mean of the National Oceanic and Atmospheric Administration (NOAA) Climate Prediction Center (CPC) MJO index (not shown) shows a strong negative MJO phase extending as far east as 120°W just prior to the January 1997 floods, consistent with the results of Mo and Higgins (1998a), but we have not performed any detailed analysis of potential links between the MJO and the Pineapple Express event in this case.

b. Synoptic overview

The large-scale flow during the event is summarized in Fig. 2. The 500-hPa height field on 24 December (Fig. 2a), prior to the main flooding event, is characterized by a weak ridge over the eastern Pacific and western North America and a strong low over Hudson Bay. By 1 January (Fig. 2b), the Hudson Bay low had moved to the east, along with the weak ridge, and a southwesterly flow had developed in the east Pacific between Hawaii and the west coast of the United States.

A surface low pressure center, located well offshore before the onset of the main flooding event (Fig. 3a), moved to just offshore of Washington by 1 January (Fig. 3b) as a low-level southwesterly flow developed along the west coast of the United States from southern California to the Canadian border. Eastward migration of a wave in the low-level temperature field brought warm air to California (Fig. 3b), raising freezing levels to an altitude of more than 3.5 km in the Sierra Nevada by 1 January. On 3 January, a weak cold front passed through the region and snow levels dropped down to an altitude of 2 km as a colder northwesterly flow developed (Fig. 3c). A sounding from Oakland (Fig. 4a) illustrates the low-level south-southwesterly flow and the relatively high freezing level at this location at 1200 UTC on 1 January 1997.

Figure 5, showing the 700-hPa wind vectors and water vapor mixing ratio (q_v), illustrates that southwesterly winds advected moisture from the central Pacific to western North America on 30 December, and that q_v reached a maximum over northern and central California on 1 January (Figs. 5a,b). By 3 January (Fig. 5c), the plume of high q_v air had migrated to the south as winds in California shifted from the southwest to the west. The advection of water vapor from the southwest is particularly evident in satellite water vapor imagery (Fig. 6), which shows that by 1 January, a plume of moist air extended from near Hawaii to the west coast of North America. By 3 January, the plume had weakened and shifted farther into southern California. Finally, 3-day averages of total column water vapor (TCWV) derived from Special Sensor Microwave/Imager (SSMI) polar-orbiting satellite data (Fig. 7) un-

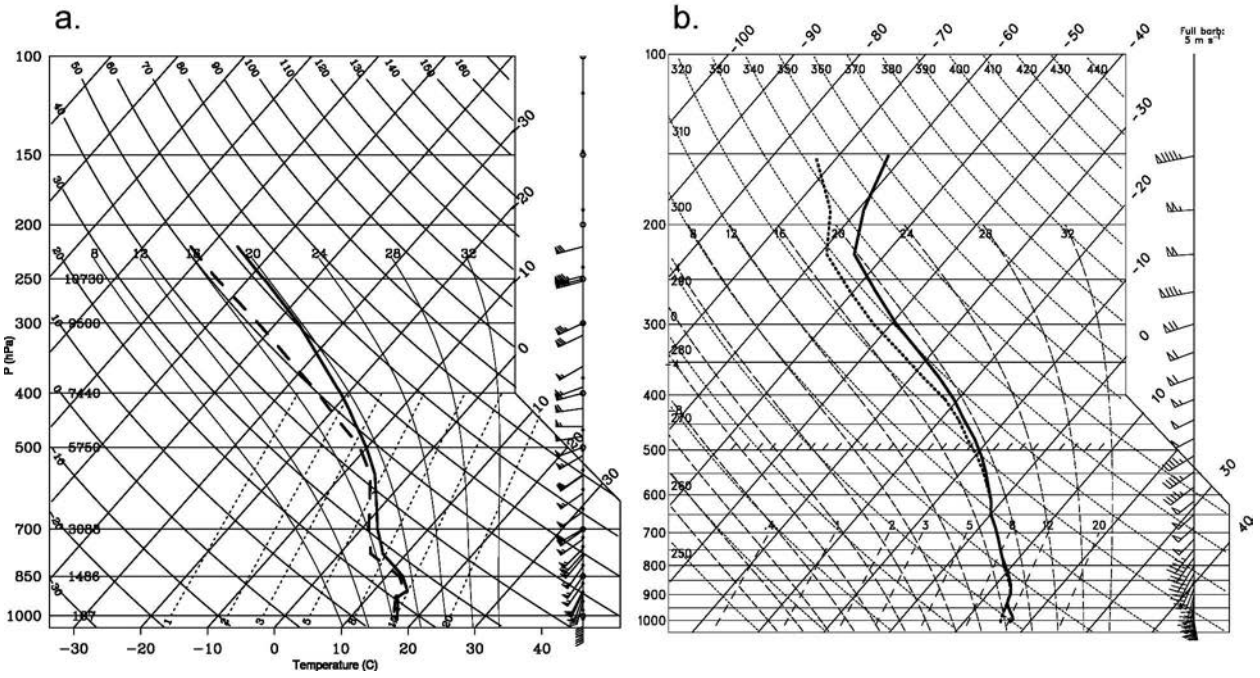

FIG. 4. (a) Observed sounding from Oakland at 1200 UTC 1 Jan 1997; (b) CTRL model sounding from Oakland at the same time and date.

ambiguously show a plume of high TCWV air emanating from the Tropics and impinging onto the west coast of the United States during this period.

c. Precipitation

The observed precipitation from 31 December 1996 through 2 January 1997 (Fig. 8) shows considerable spatial and temporal variability. The northern Sierra Nevada received significant precipitation on all three days, with a southward shift in the locus of maximum precipitation during the period, while the northern Coast Ranges received their heaviest precipitation on 1 January. Moderate rainfall occurred in the Santa Lucia Range on 2 January. Precipitation totals for this period exceeded 200 mm in many areas and even approached 700 mm in some orographically favored areas. The overall precipitation pattern is well correlated with the topography, suggesting that orographic processes likely played a significant role in localizing regions of heavy precipitation.

Hourly rainfall data (Fig. 9) show that the northern Coast Ranges (Gasquet Ranger Station site) received a pulse of heavy precipitation around 0000 UTC on 31 December, with an extended period of heavy precipitation on 1 January. The maximum hourly accumulation rate during both periods exceeded 10 mm h^{-1}. Precipitation continued throughout 2 January, but declined near the end of the day. The northern Sierra Nevada (Oroville Dam site) received a pulse of especially heavy rainfall on 1 January, with accumulation rates approaching 15 mm h^{-1}, before rainfall decreased on 2 January. The central Sierra Nevada (Mariposa site) received abundant rainfall on 1 January until early on 3 January, though the rain rates never exceeded 5 mm h^{-1}. A weak cold front passed through the region on 3 January, more than 24 h after the heaviest periods of rainfall, suggesting that frontal circulations did not play a significant role in driving the heavy rainfall.

4. Numerical model and experiment design

The numerical simulations presented here were carried out with the Pennsylvania State University–NCAR Mesoscale Model (MM5, version 3), a nonhydrostatic, primitive equation model with a terrain-following vertical coordinate (Dudhia 1993). MM5 supports multiple nested domains for higher-resolution simulation over regions of interest. All of the simulations presented here use two computational domains (Fig. 10). The outer computational domain has a horizontal grid spacing of 30 km and the inner domain has a grid spacing of 10 km. The model domains are coupled using a two-way interface and use 31 vertical levels. For our control simulation (CTRL), we use the Kain–Fritsch scheme to

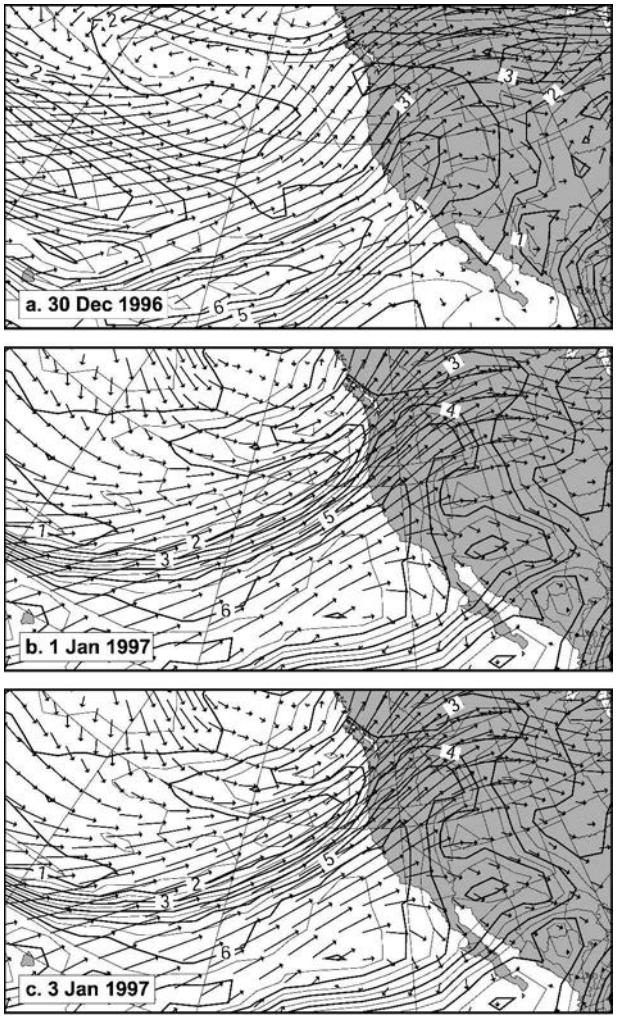

FIG. 5. NCEP–NCAR reanalysis of the water vapor mixing ratio q_v (contour interval 1 g kg^{-1}) and wind at 700 hPa on (a) 30 Dec 1996, (b) 1 Jan 1997, and (c) 3 Jan 1997. Vector scale is 1 cm = 40 m s^{-1}.

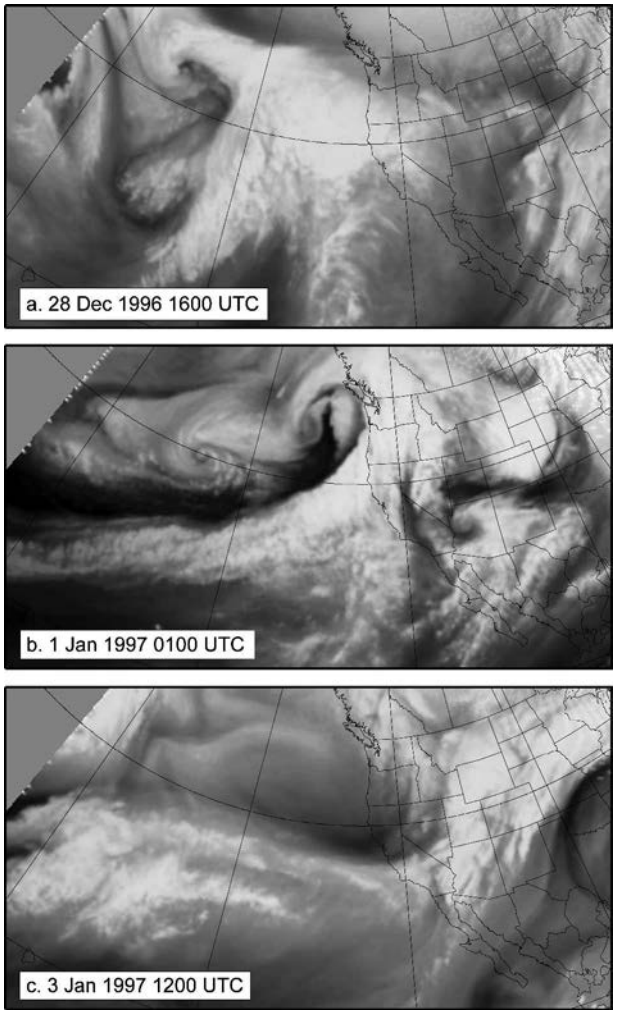

FIG. 6. *Geostationary Operational Environmental Satellite-9* (*GOES-9*) water vapor imagery on (a) 28 Dec 1996, (b) 1 Jan 1997, and (c) 3 Jan 1997.

parameterize subgrid-scale convection (Kain and Fritsch 1993). We also use the simple ice microphysics of Dudhia (1989), the Hong–Pan (1996) planetary boundary layer parameterization, and a simple five-layer soil model.

The results presented here are robust with respect to domain configuration and model resolution (both horizontal and vertical). Higher-resolution simulations (with 3.3- and 1.1-km grid spacing; not shown) resolve finer scales in the atmospheric flow and in the precipitation fields, but do not otherwise affect the interpretation presented here. Mass et al. (2002) showed that higher model resolution can lead to significant overprediction of orographic rainfall in some cases. In the case presented here, however, there was little overprediction of rainfall at higher model resolution (not shown), and since we are primarily interested in atmospheric flows on scales of a few tens of kilometers rather than the finescale features of the rainfall field, the inner domain resolution of 10 km is sufficient. The results are also largely insensitive to the microphysics parameterization. Experiments with more complex schemes (not shown) yield precipitation amounts and spatial distributions that are close to those simulated with the simple ice scheme. Although a detailed microphysics sensitivity study is beyond the scope of this paper, we believe that this relative insensitivity is due to the fact that the temperatures during the event were warm and freezing levels were high, so that the role of ice processes in this event was relatively small.

We examined the roles of topography and latent heating by carrying out additional experiments that attempted to isolate their relative effects. The role of

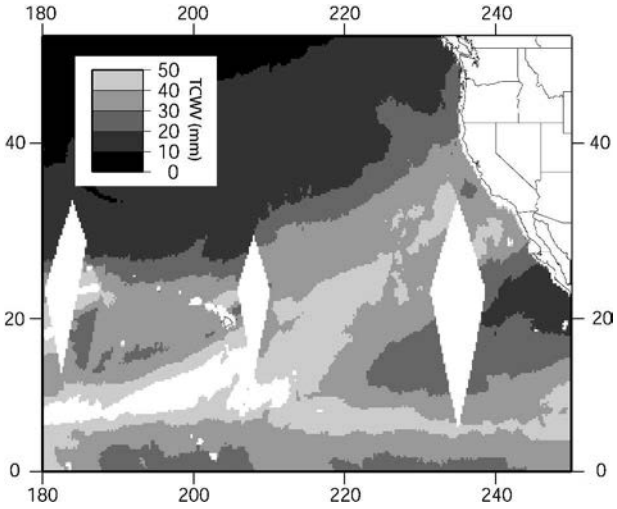

FIG. 7. SSM/I total column water vapor (mm): 3-day average from 30 Dec 1996 through 1 Jan 1997.

latent heating was assessed by running a simulation in which all latent heating was set to zero (the FDRY simulation), but in which all other parameters were the same as CTRL. We performed an additional simulation to assess the effects of topography in which all model topography was set to zero (NOTOPO).

The NCEP 40-km Eta analysis was interpolated to the MM5 Lambert conformal grid to provide the initial conditions at 0000 UTC 30 December 1996 and the 12-h boundary conditions to the 30-km outer domain. The inner domain received its lateral boundary conditions from the outer domain during the model integration. All simulations begin at 0000 UTC 30 December 1996 and end at 0000 UTC 4 January 1997.

5. Model verification

The model-simulated sea level pressure field (not shown) is in good agreement with the analyses and accurately reproduces the offshore low pressure center as well as the overall evolution of the event. Similarly, the 500-hPa geopotential height field (also not shown) is well simulated.

The overall warming that affected the High Sierra region is generally well simulated (Fig. 11), though the model tends to overestimate temperatures during the passage of the weak cold front on 2 and 3 January. The highest temperatures occurred around 0000 UTC on 2 January, and this peak is captured by the simulation. The modeled sounding from Oakland (Fig. 4b) accurately reproduces the observed temperature and wind direction, though the model is saturated over a deeper layer than was observed.

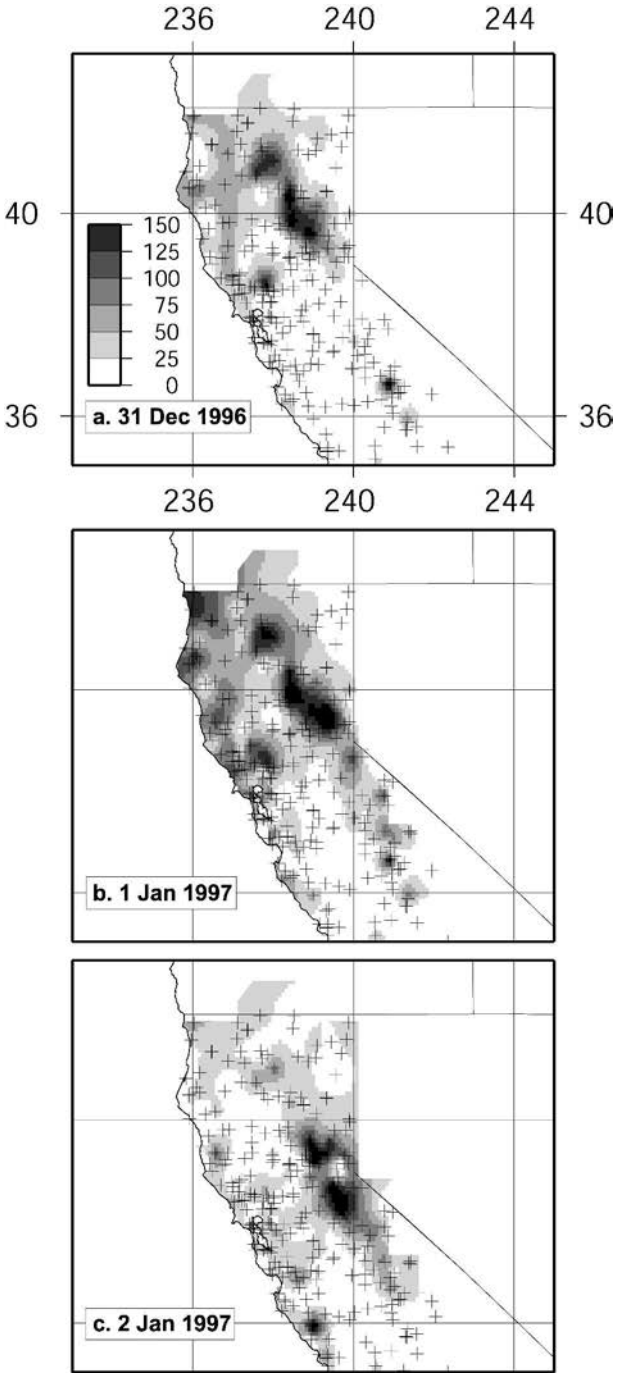

FIG. 8. Gridded observed 24-h-accumulated precipitation (mm) for (a) 31 Dec 1996, (b) 1 Jan 1997, and (c) 2 Jan 1997. Crosses indicate locations of rain gauges.

The simulated storm totals (31 December–3 January) from the 10-km domain (Fig. 12b) capture the main features of the observed precipitation (Fig. 12a), including precipitation maxima in the northern Sierra Nevada, Mount Shasta region, and northern Coast

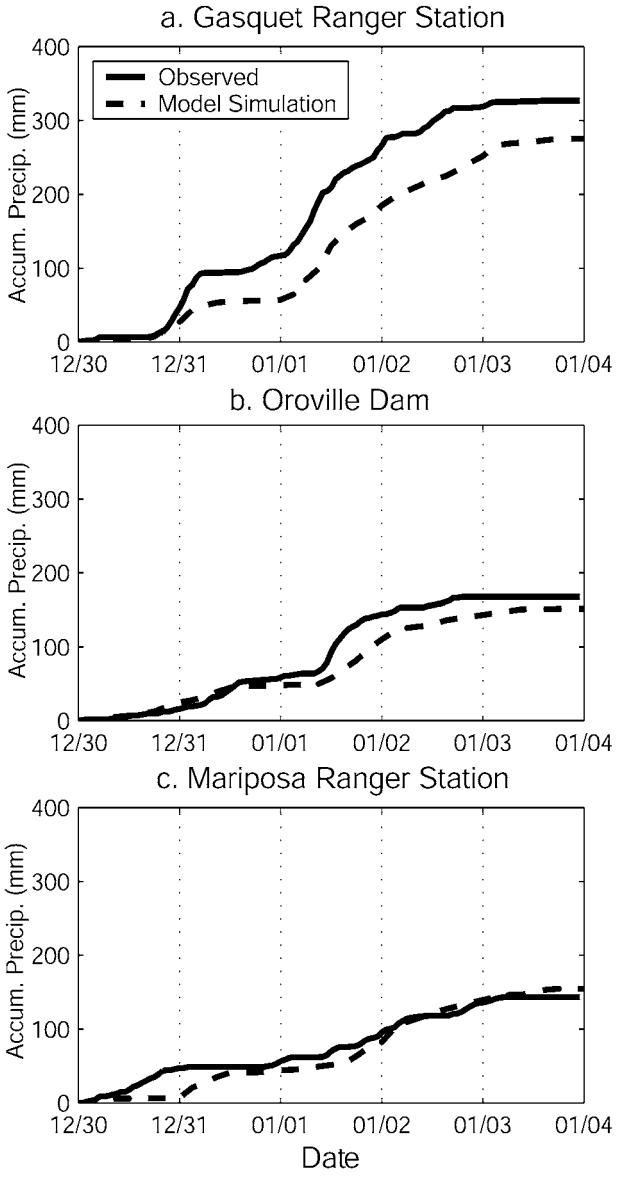

FIG. 9. Hourly observed (solid line) and 3-h CTRL simulation (dashed line) accumulated precipitation (mm). See Fig. 1 for station locations. Vertical tick marks indicate 0000 UTC.

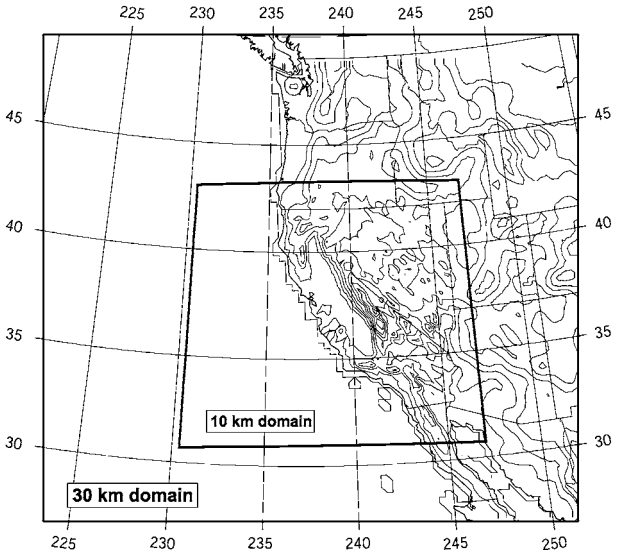

FIG. 10. Model terrain (400-m contour interval) from 30-km domain. Inner box shows location of the 10-km domain.

Ranges. The sharp decay of precipitation in the lee of the Sierra Nevada is well simulated by the model. The simulated precipitation in the Santa Lucia Range occupies a narrower zone than observed. Given the caveats regarding rain gauge data described above, the overall estimated precipitation totals compare favorably with the observational network.

The model underestimates the precipitation on 31 December (Fig. 13; see Fig. 9 for the daily observations), though it does accurately capture maxima in the northern Sierra Nevada and south of Mount Shasta. The 1 January simulation is generally better than that from 31 December, with rainfall maxima in the northern Sierra Nevada, Mount Shasta, and heavy rainfall throughout Coast Ranges north of San Francisco. The model accurately simulates the southward shift in maximum precipitation on 2 January.

The model results generally match the timing and total accumulation of precipitation observed at the hourly rain gauge stations (Fig. 9), though they underestimate the pulse of heavy rainfall observed at the Gasquet Ranger Station site (northern Coast Range) at 0000 UTC on 31 December. The model does capture both the timing and magnitude of the precipitation on 1 January at both the Gasquet and Oroville sites, and precipitation at the Mariposa Ranger Station is generally well simulated throughout the event.

6. Analysis and sensitivity experiments

a. Control experiment

Having reviewed the overall ability of the MM5 to simulate the January 1997 event, we now use model results to investigate the dynamics that controlled the distribution of precipitation during the 31 December–2 January time frame. We focus on the relationship between near-surface winds (at $\sigma = 0.95$) and lower-tropospheric winds (at 700 hPa) and the distribution of equivalent potential temperature (θ_e) in the northern Coast Ranges, the Santa Lucia Range, the Central Valley, and the Sierra Nevada Range.

The simulated winds and θ_e are summarized in Figs. 14 and 15. The $\sigma = 0.95$ flow offshore of the northern Coast Ranges was dominated by relatively high θ_e and

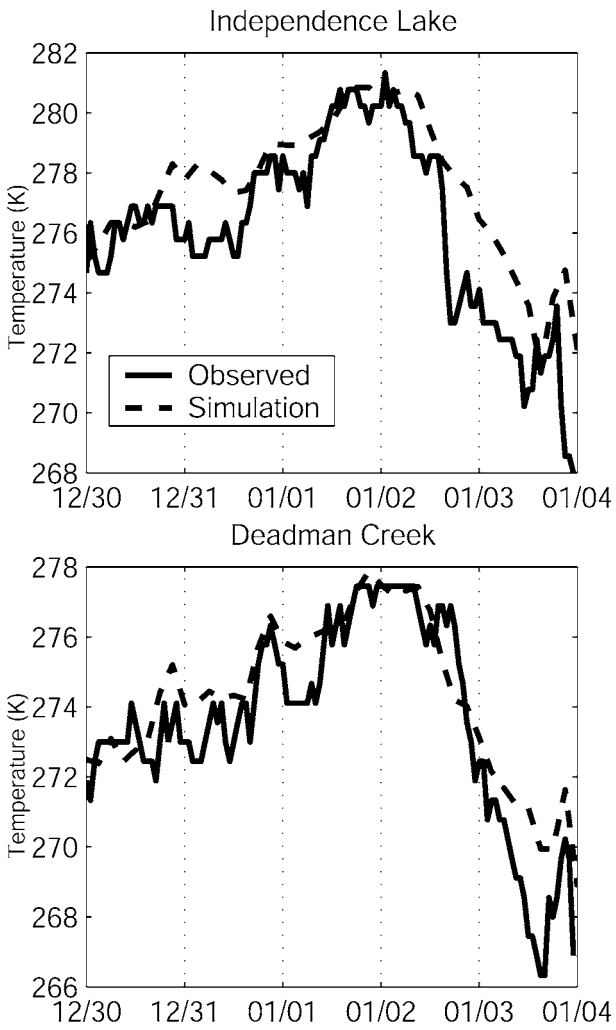

FIG. 11. As in Fig. 9, but for surface temperature (K).

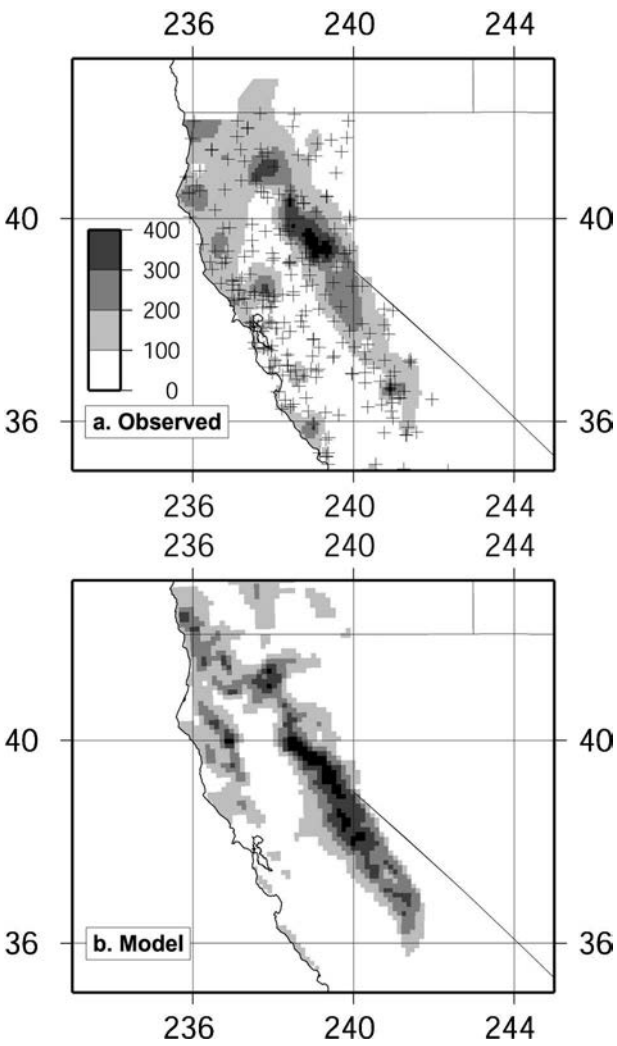

FIG. 12. Total accumulated precipitation (mm) 0000 UTC 31 Dec 1996–0000 UTC 4 Jan 1997. (a) Observed rain gauge data; (b) 10-km-resolution CTRL model.

strong south-southwesterly winds on 31 December and 1 January. In contrast, the $\sigma = 0.95$ winds offshore of the Santa Lucia Range on the central coast were roughly parallel to the coast and marked by sharp gradients in θ_e on 31 December and 1 January. On 2 January, the low-level winds shifted to a southwesterly direction, with relatively high values of θ_e impinging upon the central coast.

The $\sigma = 0.95$ winds in the Central Valley were parallel to the topography of the Sierra Nevada and were characterized by low θ_e air on 31 December and 1 January (the NNW–SSE-oriented light tongue in the center of the two left-hand plots). By 2 January, rising values of θ_e in the Central Valley and decay of the mountain-parallel winds accompanied increased precipitation in the central and southern Sierra Nevada. On 3 January, the high θ_e air had moved to the south and weak flows predominated.

The 700-hPa winds were generally more uniform throughout the event and were dominated by advection of high θ_e air from the southwest on 1 January. The heaviest rainfall in the northern Sierra Nevada occurred on 1 January, when the high θ_e air at 700 hPa was transported over the lower θ_e air that was advected from the south.

The vertical structure in the northern Central Valley and northern Sierra Nevada during this period is shown in Fig. 16 and further illustrates this point. During the period of heaviest rainfall in this region (Fig. 16a) at 1800 UTC on 1 January, w had a maximum value in excess of 70 cm s^{-1} on the windward slope above a steep blanket of lower θ_e air. Above this low-level air, the vertical stratification of θ_e was weak. By 1800 UTC on 2 January (Fig. 16b), the winds in the Central Valley

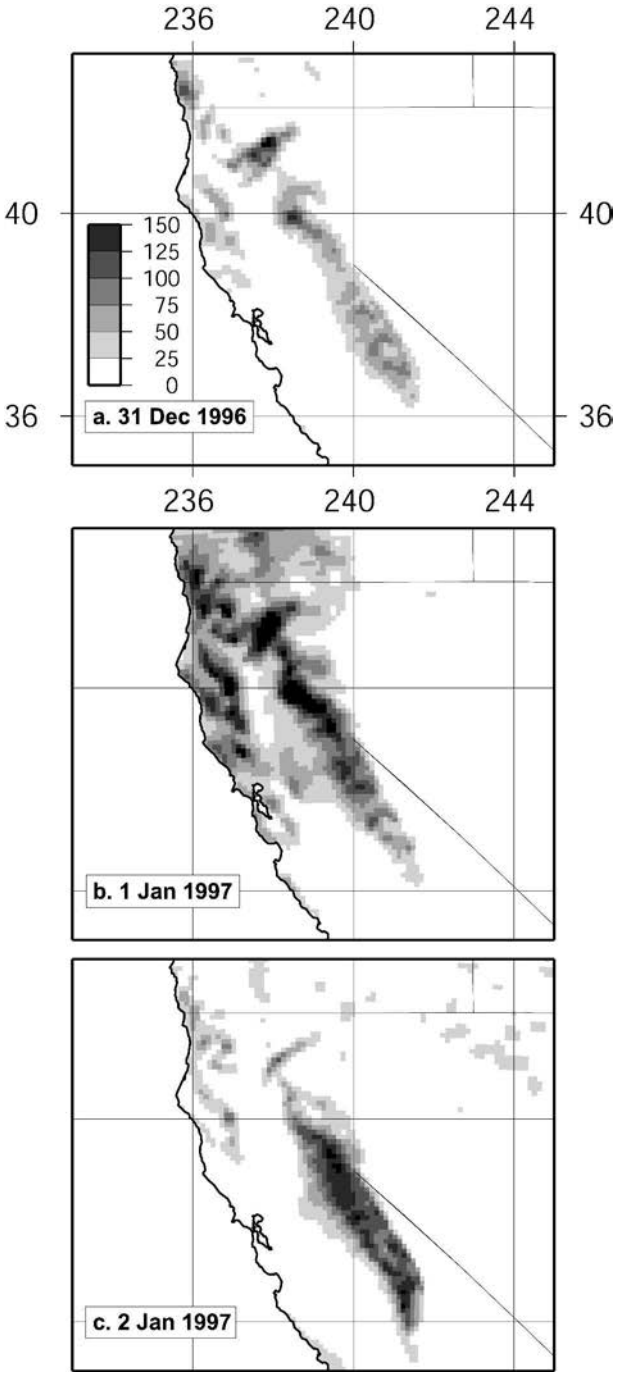

FIG. 13. The 24-h-accumulated precipitation (mm) from 10-km-resolution CTRL model for (a) 31 Dec 1996, (b) 1 Jan 1997, and (c) 2 Jan 1997.

were no longer exporting lower θ_e air to the north, and the entire troposphere along this cross section had lower values of θ_e than on 1 January. The maximum w was reduced by half from the previous day and shifted somewhat lower, to just above the windward slope.

The vertical structure along the central coast and central Sierra Nevada is illustrated in Fig. 17. At 0600 UTC on 1 January (Fig. 17a), alongshore winds transported low θ_e air along the steep Santa Lucia Range front and in the Salinas Valley. Similar conditions had developed in the Central Valley. There was relatively little precipitation in this region on 1 January, but by 1200 UTC 2 January (Fig. 17b), the mountain-parallel winds were replaced by a strengthening onshore flow and the low θ_e air had been replaced by higher θ_e air at the lowest levels. Vertical velocities, which had been weak on 1 January, exceeded 30 cm s^{-1} along the central coast and 50 cm s^{-1} on the windward slope of the Sierra Nevada.

The time evolution of relative humidity at three locations is shown in Fig. 18. On 1 January, the atmosphere offshore of the northern Coast Ranges was saturated below 800 hPa, while the Central Valley and the coastal region of the Santa Lucia Range were unsaturated at low levels. By 2 January, however, this situation had changed, with deep saturation in the Central Valley and coastal Santa Lucia Range and diminishing relative humidity aloft near the northern Coast Ranges. During the periods of deep saturation in each region, the winds were able to flow over topographic barriers, suggesting the possibility that latent heat release during condensation may have lowered the effective static stability during those periods.

The model results indicate that the atmospheric flows during this event were characterized by winds that were sometimes parallel to topographic barriers and sometimes oblique to those barriers, suggesting a complex combination of flow-over and flow-around processes. We now attempt to disentangle the relative roles of topography and latent heating by considering two numerical experiments, one with all model topography set to zero (NOTOPO) and another without latent heating (FDRY).

b. Experiment without topography

The low-level ($\sigma = 0.95$) θ_e field in NOTOPO (Fig. 19) was characterized by northwest–southeast lateral gradients, ranging (on 1 January) from a high of around 330 K in far northern California to a low of around 315 K offshore southern California. The overall pattern shifted to the southeast over time. The maximum in θ_e corresponded to a maximum in q_v (not shown) of around 12 g kg^{-1} that decayed toward the southeast to about 5 g kg^{-1}.

The low-level ($\sigma = 0.95$) winds for the NOTOPO case are shown in Fig. 19. In the NOTOPO case, there was little flow deflection either along the coast or in the Central Valley. On 31 December and 1 January, rela-

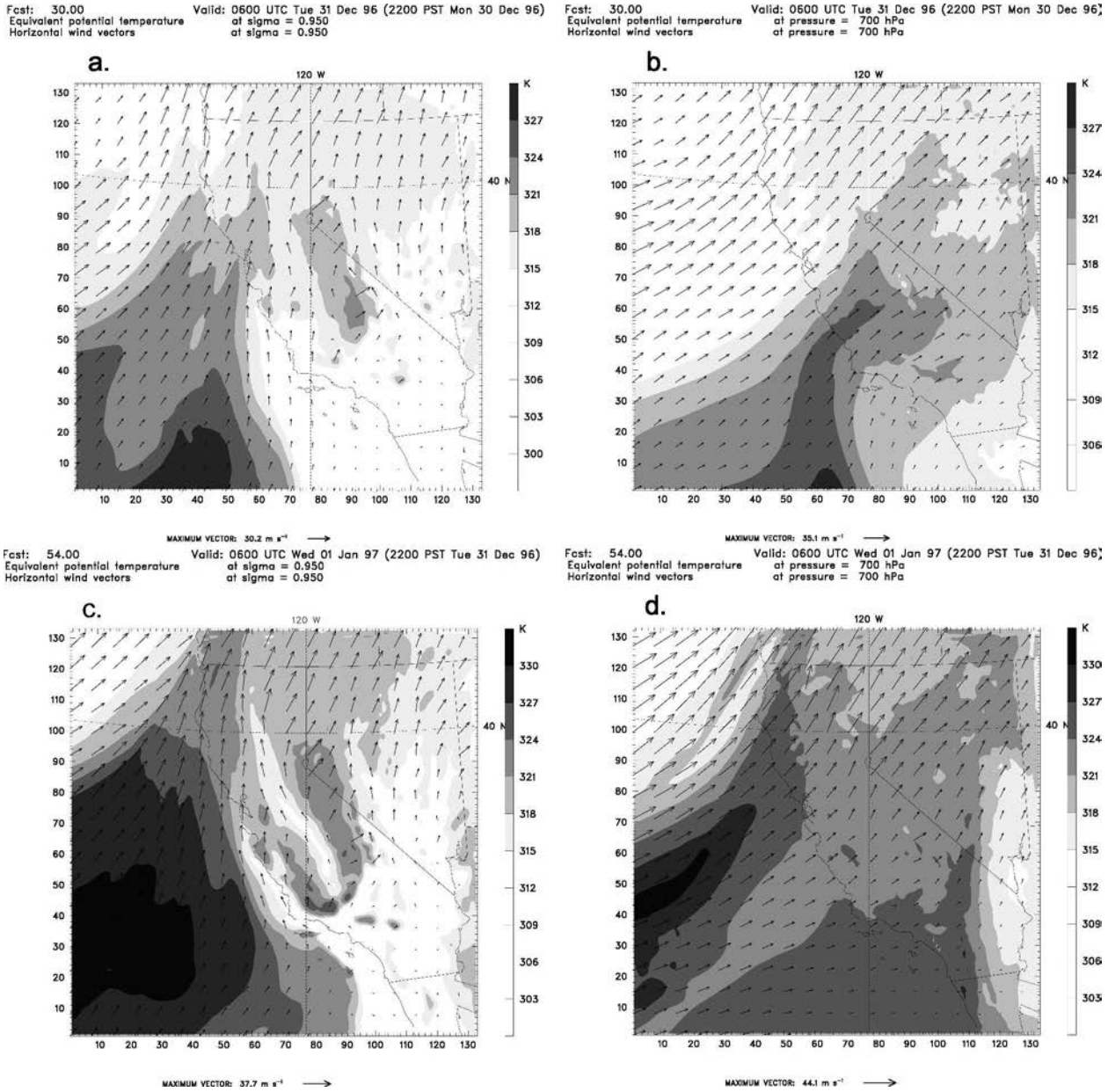

FIG. 14. CTRL simulated horizontal wind vectors and θ_e (grayscale) at (a), (c) $\sigma = 0.95$ and (b), (d) 700 hPa on (a), (b) 31 Dec 1996 and (c), (d) 1 Jan 1997. Wind vectors are scaled so that a vector representing 30 m s^{-1} exactly reaches the tail of the next adjacent vector.

tively high θ_e air was transported across the Central Valley, in a region dominated by low θ_e air in CTRL on that date, suggesting that low-level blocking by the Coast Ranges prevented relatively high θ_e air from reaching the Central Valley in CTRL.

The low-level winds in NOTOPO help to illuminate the relative degree of blocking in CTRL. The winds offshore of the Santa Lucia Range in NOTOPO on 1 January are southwesterly, while the winds in CTRL are weaker and more southerly. On 2 January, the low-level winds are much stronger in NOTOPO than in CTRL even though the orientations are the same. These observations suggest that the upstream influence of the Santa Lucia Range extended well offshore on 1 January. On 2 January, in contrast, the coastal winds in CTRL are not blocked, though the winds are apparently weakened by the presence of the topographic barrier.

The nondimensional parameters relevant to understanding the influence of topography on the low-level

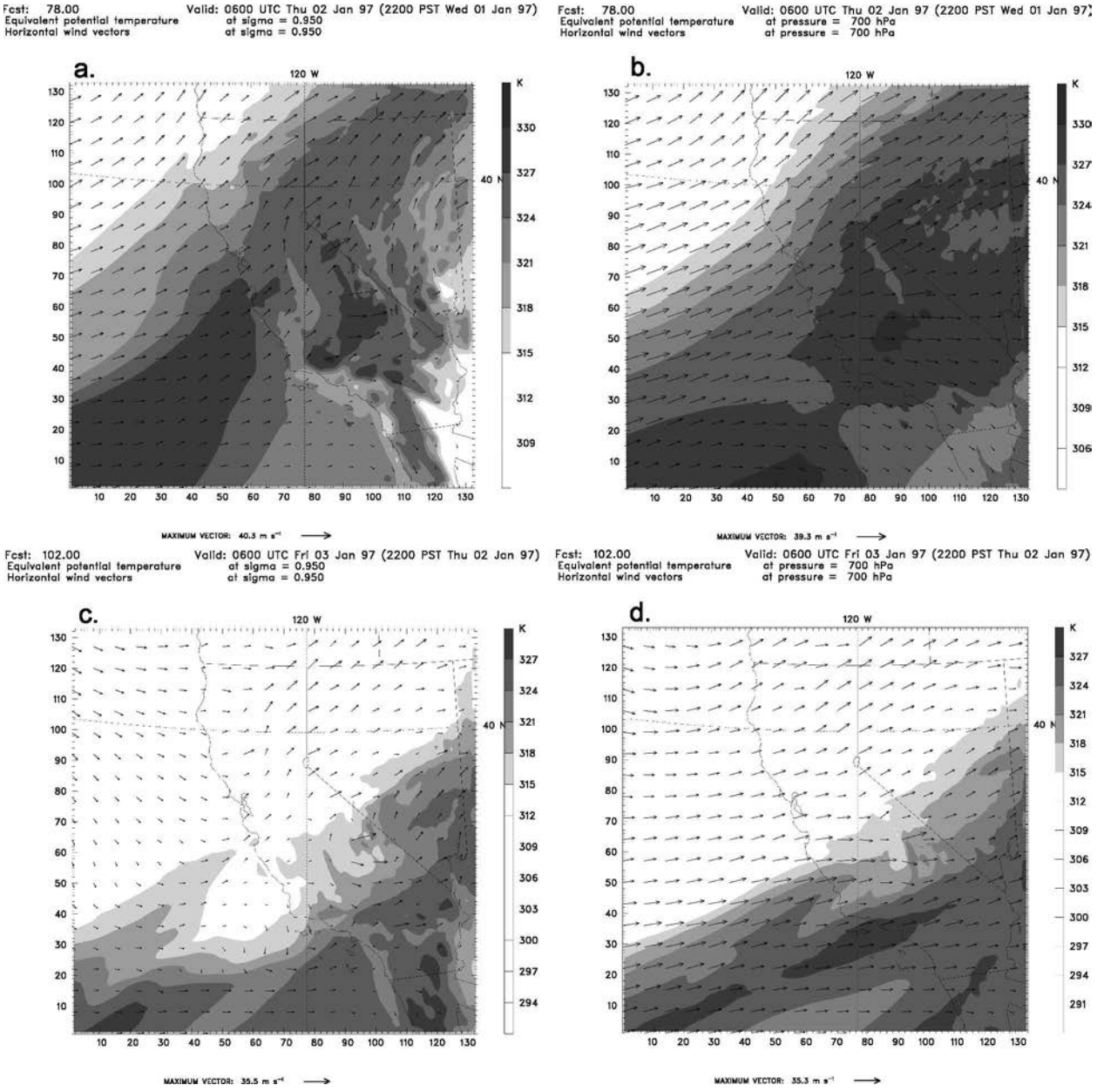

FIG. 15. As in Fig. 14, but for (a), (b) 2 Jan 1997 and (c), (d) 3 Jan 1997.

flow can be diagnosed from the NOTOPO simulation. We focus here on 0600 UTC 1 January 1997, a period of apparently significant blocking offshore of the Santa Lucia Range in CTRL. From NOTOPO, we estimate the undisturbed flow normal to the topography in a layer from the surface to the mountain top (at about 1000 m) to be about 8–10 m s^{-1}; N is about 1.4×10^{-2} s^{-1}, yielding $U/hN \approx 0.6$, indicating that the flow parameters near the topography of the Santa Lucia Range lay in the nonlinear regime. The extent of the upstream effect can be estimated by the Rossby radius of deformation, $Nh/f \approx 150$ km. Analysis of the difference between CTRL and NOTOPO low-level winds (not shown) indicates that the upstream effects do extend about 200 km offshore, indicating that the CTRL model results do generally agree with the basic theory for flow blocking and the upstream influence of topography.

Vertical velocities in the NOTOPO experiment (not shown) never exceeded about 2 cm s^{-1}, indicating that most of the uplift during this event, and thus most of the precipitation, was due to orographic forcing and not to large-scale uplift. Consequently, the total precipitation

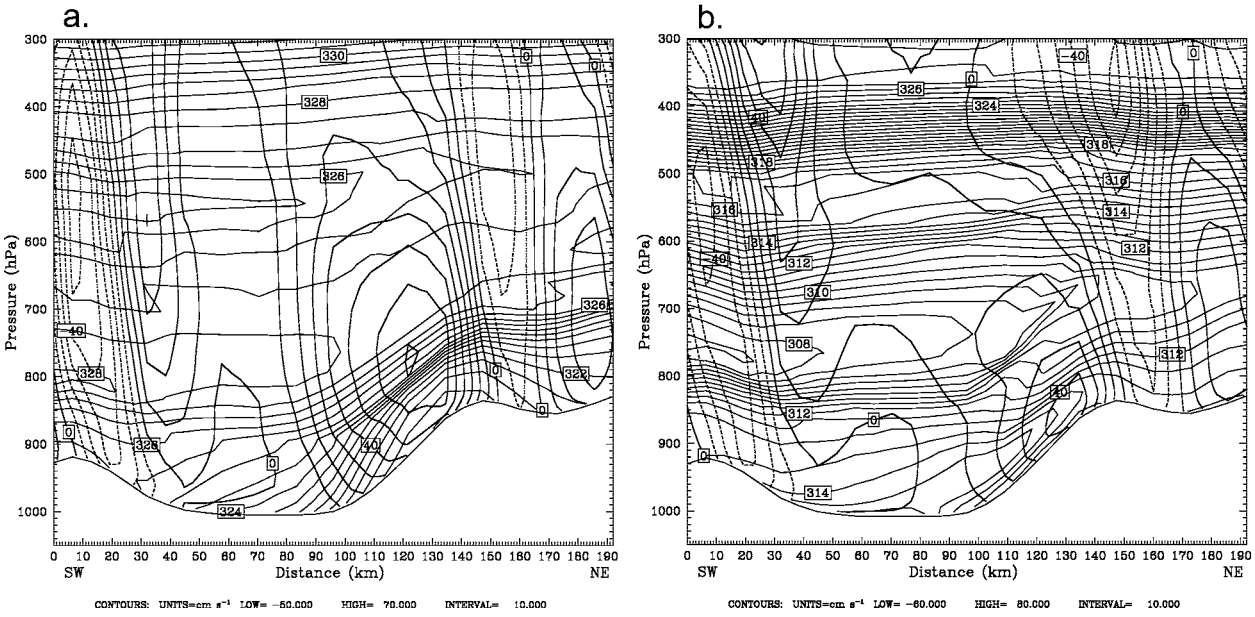

FIG. 16. CTRL profile of θ_e (thin contours; contour interval 0.5 K) and w (heavy contours; contour interval 10 cm s^{-1}) for northern Sierra Nevada at (a) 1800 UTC 1 Jan 1997 (the period of heaviest rainfall) and (b) 1800 UTC 2 Jan 1997. See Fig. 1 for location.

for the NOTOPO case (not shown) nowhere exceeded 60 mm and was thus an order of magnitude lower than CTRL.

The low-level winds in NOTOPO were relatively undeflected compared to CTRL, indicating that the low-level CTRL winds in the Central Valley and along the central coast were blocked by the mountainous topography on 31 December and 1 January, but not on 2 January. The topography of the northern Coast Ranges, however, did not cause significant deflection of the low-level winds in that region during the event (see Fig. 14c). In general, it appears that winds transporting relatively high θ_e were able to flow over topographic barriers, while lower θ_e winds were blocked.

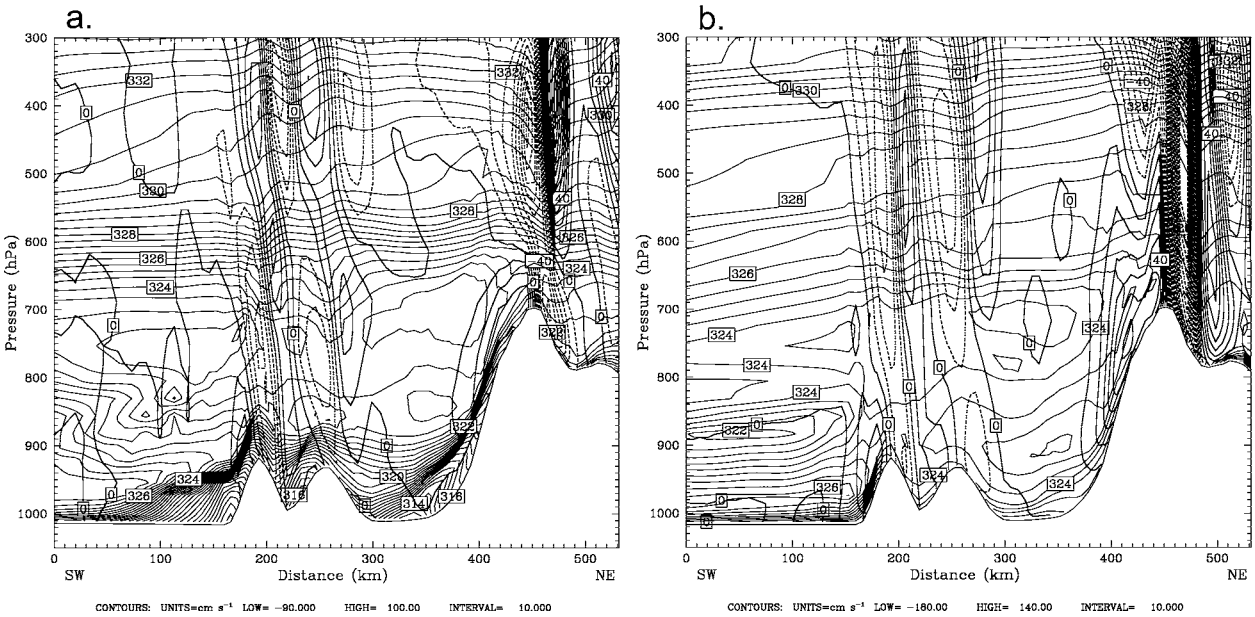

FIG. 17. As in Fig. 16, but for southern Sierra Nevada at (a) 0600 UTC 1 Jan 1997 and (b) 1200 UTC 2 Jan 1997. Different times are selected to highlight the transition from blocked to unblocked flow. See Fig. 1 for location.

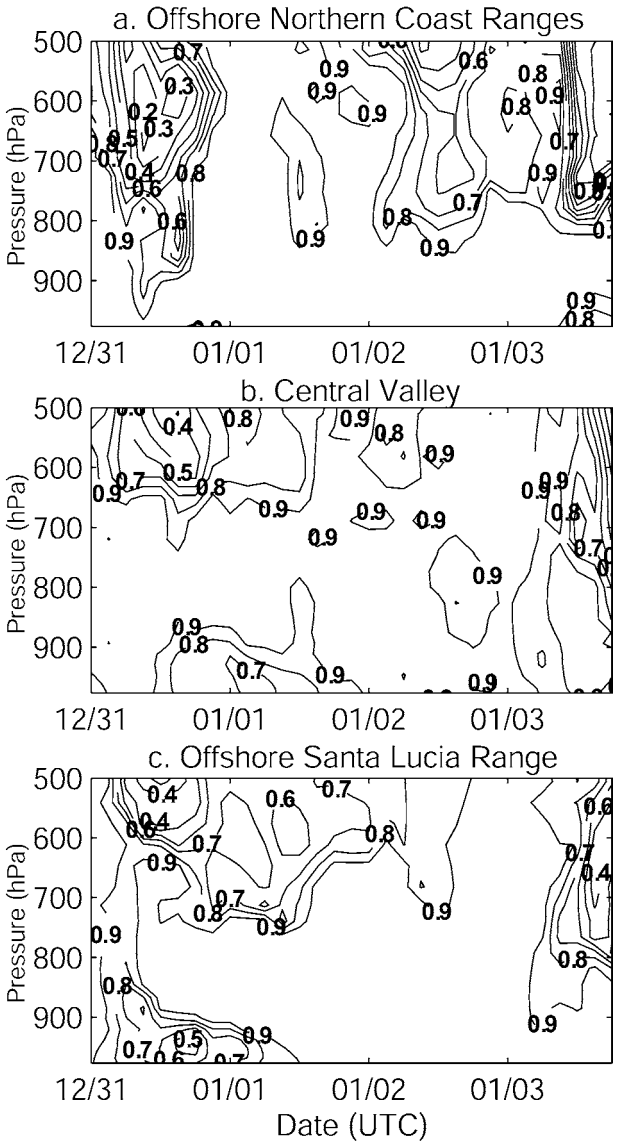

FIG. 18. Time–height evolution of relative humidity in CTRL at three locations: (a) just offshore of the northern Coast Ranges; (b) in the Central Valley; and (c) just offshore of the Santa Lucia Range. See Fig. 1 for location of sites.

c. *Experiment without latent heating*

The $\sigma = 0.95$ winds for the FDRY case are shown in Fig. 20. The winds just offshore of the northern Coast Ranges were much more deflected than in CTRL on 2 January, while the winds in the Central Valley remained parallel to the Sierra Nevada, even in the presence of high θ_e air. Unlike CTRL, the winds offshore of the Santa Lucia Range remained deflected on 2 January in FDRY. The θ_e field in FDRY was generally characterized by more pronounced coastal gradients than in CTRL, particularly offshore of the Santa Lucia Range on 2 January. The northern Coast Ranges had generally lower values of θ_e in FDRY than in CTRL.

The precipitation for FDRY and its relationship with CTRL is shown in Fig. 21. The central and southern Sierra Nevada received much less precipitation in FDRY, as did inland regions of the Coast Ranges and the coastal regions of the Santa Lucia Range (Fig. 21b). In contrast, the region just offshore of the Coast Ranges received substantially more precipitation in FDRY, as did the northern Central Valley (Fig. 21c).

The timing and depth of saturation in FDRY (not shown) was very similar to that shown in Fig. 18, indicating that latent heat release was essential for the observed winds and precipitation. In the absence of latent heating, the winds were largely blocked by the mountainous topography and more precipitation fell windward of the coastal topographic barrier. Similarly, the winds were unable to surmount the southern Sierra Nevada without the reduced stability that accompanies latent heating. The winds were therefore blocked in this region and the precipitation fell in the northern Central Valley. For a straight ridge, we might expect that the flow would simply go around the ridge and that little precipitation would fall. However, because the northern Central Valley is enclosed on three sides by high topography, convergence was forced by the southerly winds and enhanced the precipitation here. Overall, the FDRY results are consistent with the idealized modeling studies of Jiang (2003), who found that turning off latent heating acted to increase the effective width of the terrain and expand the precipitation area over the windward mountain slopes.

In addition to the stability effects described above, latent heating associated with heavy precipitation can also generate low-level PV maxima that can enhance the low-level jet, which can, in turn, enhance the moisture transport (Lackmann 2002). In the absence of this latent heat feedback, the low-level jet is weaker, thereby reducing the horizontal velocity and lowering the Froude number while also reducing the moisture flux. Figure 22 illustrates the enhanced onshore winds in CTRL and associated enhancement in water vapor mixing ratio, relative to FDRY, offshore of the northern Coast Ranges on 1 January 1997, suggesting that such a mechanism may have been active during the 1997 event. A full diagnosis of PV anomalies and associated winds may help to further elucidate this feedback, but is beyond the scope of the present work.

7. Discussion

The experiments described above suggest how topography and latent heating interacted during this event.

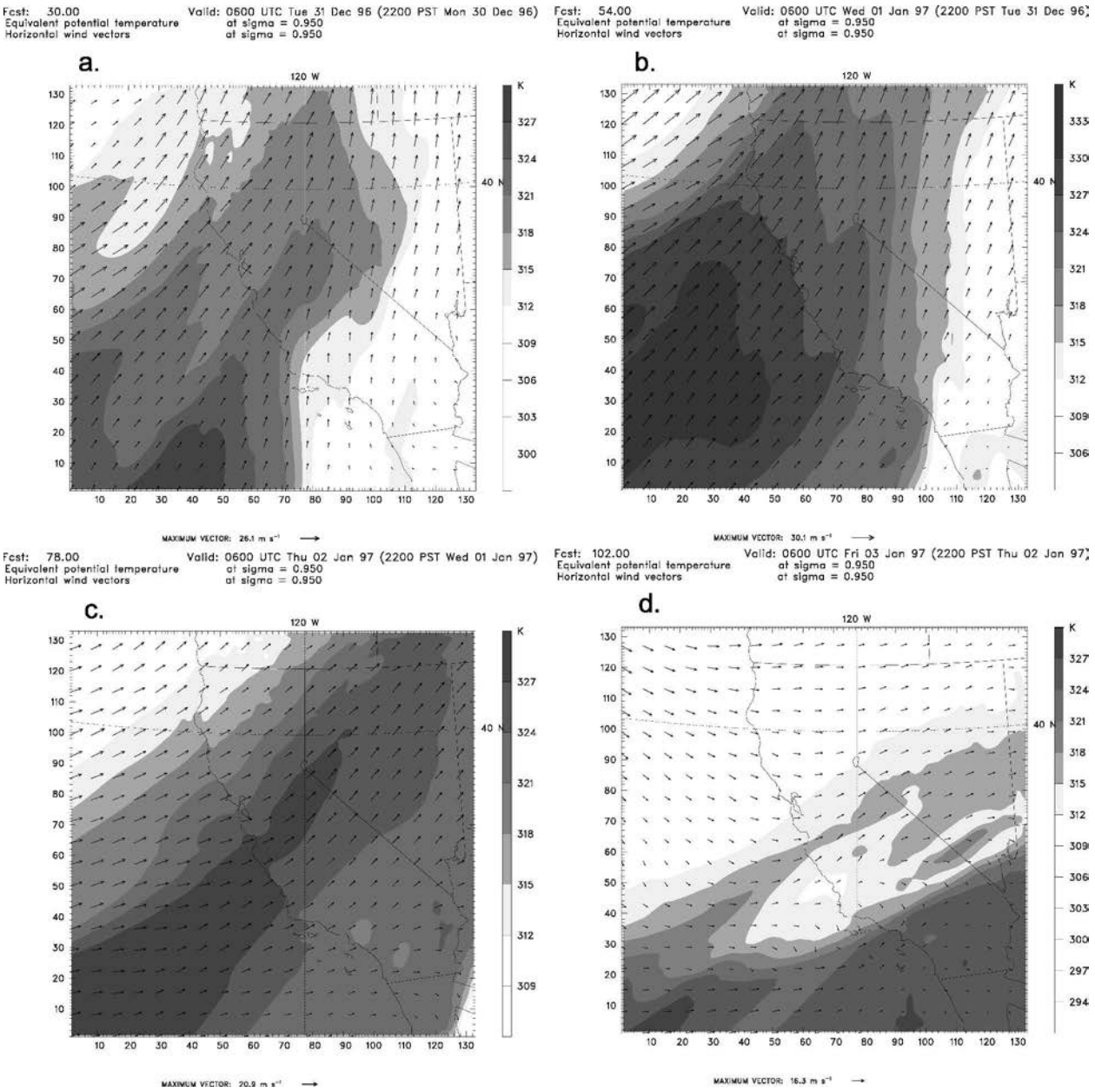

FIG. 19. As in Fig. 16, but for NOTOPO at $\sigma = 0.95$ only on (a) 31 Dec 1996, (b) 1 Jan 1997, (c) 2 Jan 1997, and (d) 3 Jan 1997.

On 1 January, the north–south distribution of atmospheric stability supported low-level flow blocking in the southern Central Valley and offshore of the Santa Lucia Range, while orographic uplift was favored offshore of the northern Coast Ranges. Low θ_e air flowed into the northern Central Valley from the south in a range-parallel jet and created a blanket of low θ_e air over which moist air was uplifted, creating heavy rainfall in that region.

As the event evolved, the core of the moist air shifted to the south. By 2 January, the atmosphere along the Central Coast and in the southern part of the Central Valley had become saturated, thus favoring orographic uplift, rather than blocking, due to the reduced stability accompanying latent heat release in the saturated air. Uplift continued in the northern Sierra Nevada, though the geometry of uplift had changed because of the decay of the barrier jet.

Some aspects of the dynamics of the 1997 California flood were similar to those in the 1994 Piedmont flood in Italy (Buzzi et al. 1998; Ferretti et al. 2000). Rotunno and Ferretti (2001) performed idealized simulations of

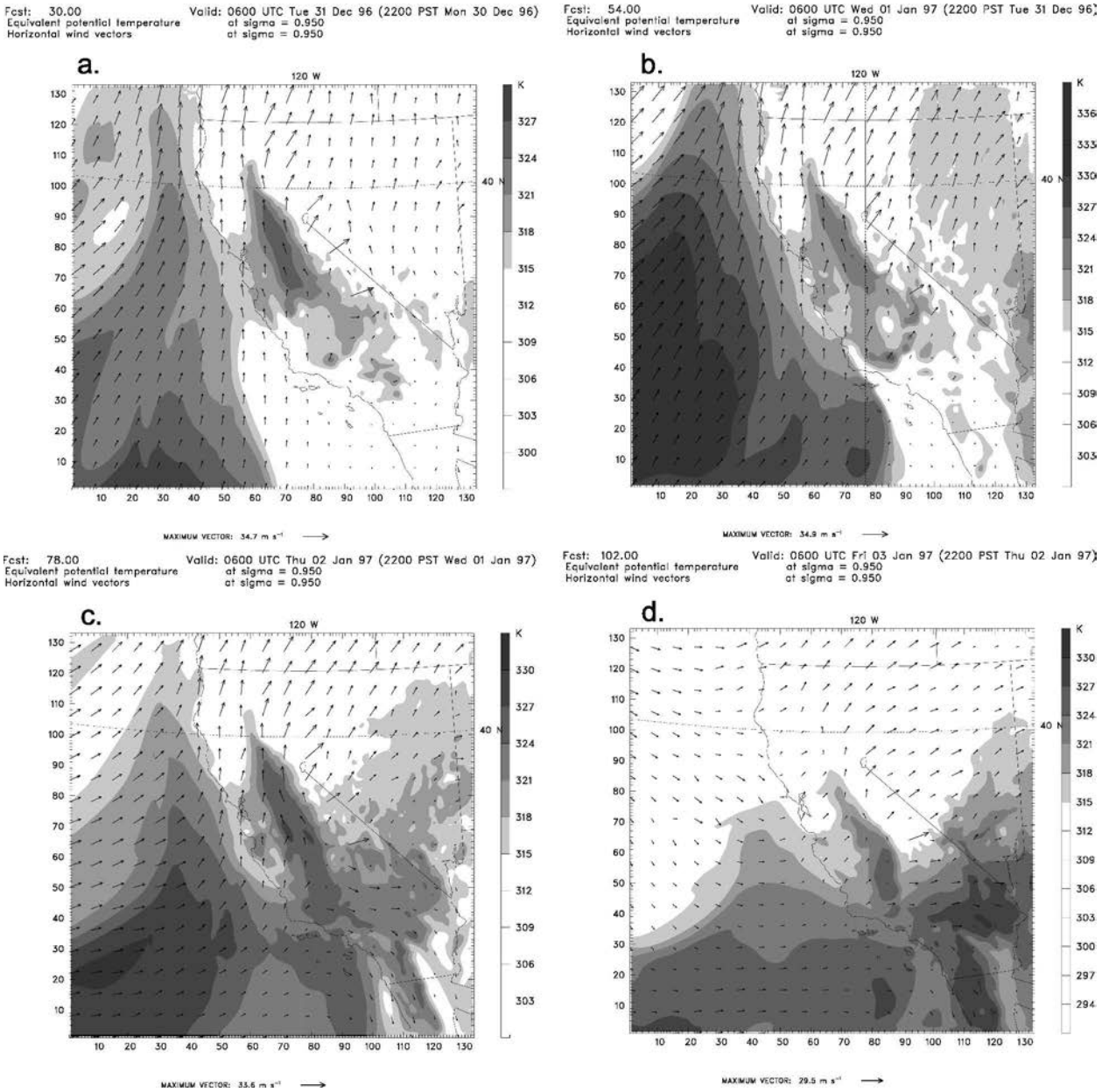

FIG. 20. As in Fig. 19, but for FDRY simulation.

the interaction of a moist flow with Alpine topography and recognized that the horizontal moisture gradient was a key factor in the precipitation during that event. The convergence between deflected, low θ_e air and undeflected high θ_e air was essential for producing the high rain rates observed. They found that the blanket of low-level, low θ_e air effectively steepened the topography over which the moist, midlevel air flowed, thereby increasing vertical velocities and local rain rates.

Unlike the Piedmont flood, the California event was almost entirely orographically driven, with minimal large-scale uplift. On the other hand, it was similar to the Piedmont case in that the horizontal moisture gradient controlled the distribution of static stability in such a way as to lead to convergence between blocked and unblocked flow, particularly on 1 January. In the southern portions of the Central Valley, the moist static stability was relatively high due to low θ_e air at the surface. The flow was thus blocked there, and a barrier jet developed. This barrier jet of low θ_e air impinged on higher θ_e air to the north. This higher θ_e northern air mass had sufficiently low moist stability to flow over the

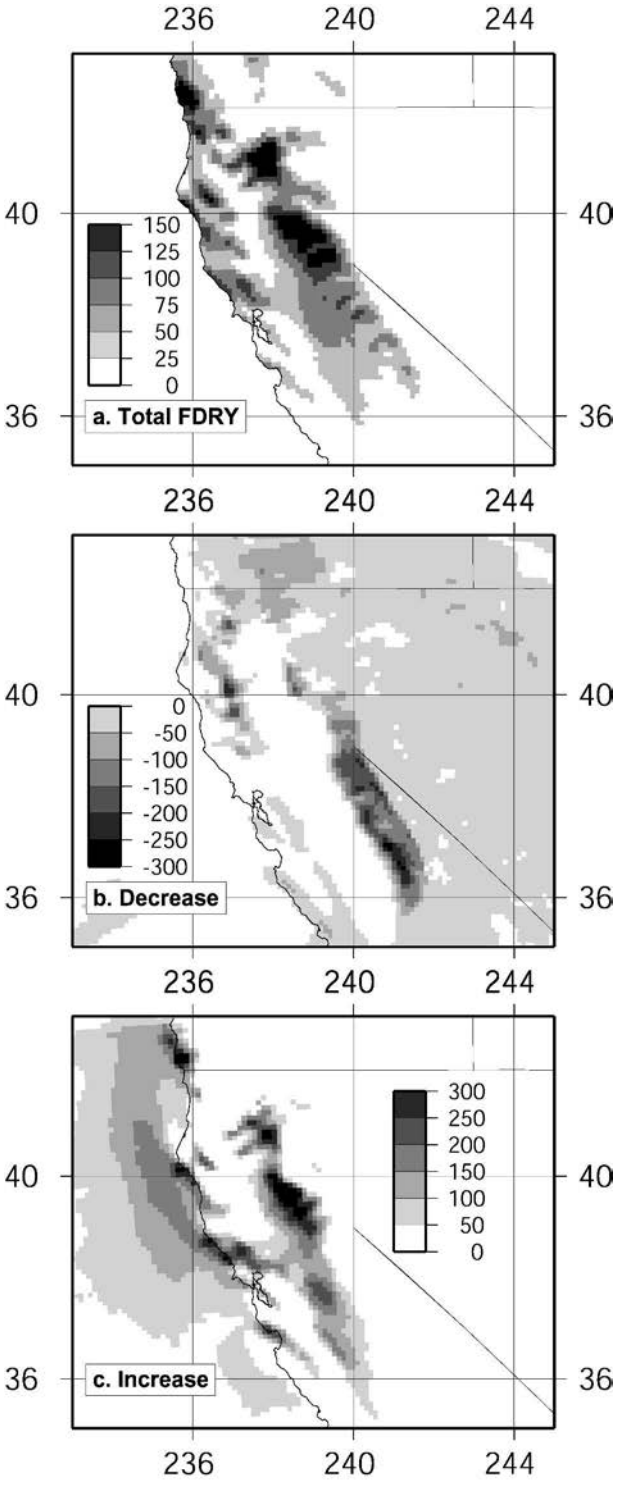

FIG. 21. Precipitation from FDRY (mm): (a) total, (b) decrease relative to CTRL for 31 Dec 1996–4 Jan 1997, and (c) increase relative to CTRL for the same time period.

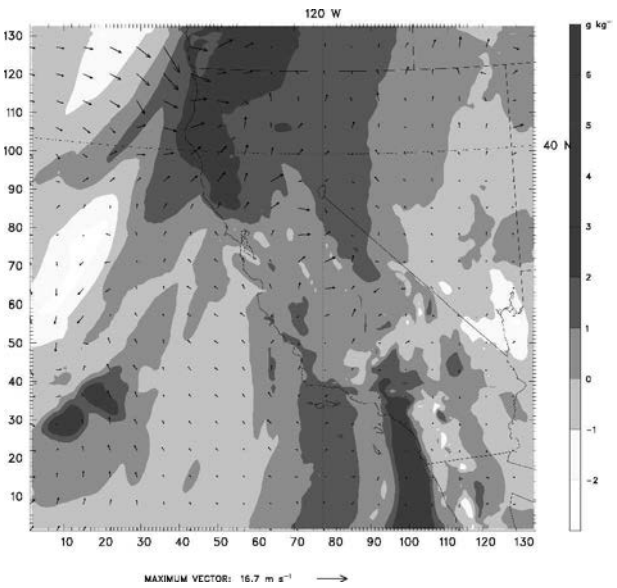

FIG. 22. Difference between CTRL and FDRY fields at 850 hPa for winds (vectors) and water vapor mixing ratio (grayscale) at 0600 UTC 1 Jan 1996, illustrating enhanced onshore flow and water vapor mixing ratio for CTRL, relative to FDRY, along the northern Coast Ranges.

topographic barrier, due to the effective static stability reduction from latent heat release. The dynamical convergence and effective topographic steepening due to the impinging low θ_e air from the south enhanced rain rates where the two air masses met. The southward propagation of the moist plume changed the low-level flow later in the event, thus bringing heavy precipitation to the southern Sierra Nevada on 2 and 3 January.

Even in the absence of moisture, a version of the Rotunno–Ferretti mechanism could operate if a sufficient horizontal gradient of dry static stability were present. In the present case, inspection of the near-surface temperature and humidity fields separately (not shown) indicates that the θ_e of the blocked air flowing northward along the topographic barrier on 1 January was lower than the unblocked air to the north on which it impinged, largely due to lower humidity rather than to lower temperature. Thus moist effects appear to have played a major role in the dynamics of this event.

8. Summary

We have presented a case study of the January 1997 "Pineapple Express" event in California using numerical simulations. The conclusions of this analysis, based on model output, observations, and sensitivity experiments, are as follows: 1) the heavy precipitation during this event was largely controlled by the interaction of

the flow with mountainous topography, with little contribution from large-scale uplift; 2) latent heating during uplift and condensation within saturated zones of the flow was essential for lowering the effective stability and enhancing uplift over mountainous terrain, particularly in the northern Coast Ranges, and for enhancing the low-level jet and associated moisture transport; 3) the horizontal configuration of static stability played a key role in the event by setting up a complex combination of flow-over and flow-around regimes that enhanced uplift in the northern Sierra Nevada during the period of heaviest rainfall.

Acknowledgments. This research was supported by NASA Grant NNG04GA73G. Use of the MM5 was made possible by the Microscale and Mesoscale Meteorology Division of the National Center for Atmospheric Research (NCAR), which is supported by the National Science Foundation. We thank Gerard Roe (University of Washington), Brian Colle (Stony Brook University), David Kingsmill (University of Colorado), Richard Rotunno (NCAR), and three anonymous reviewers for helpful discussions.

REFERENCES

Barcilon, A., J. Jusem, and P. Drazin, 1979: On the two-dimensional hydrostatic flow of a stream of moist air over a mountain ridge. *Geophys. Astrophys. Fluid Dyn.,* **13,** 125–140.

Bell, G., and L. Bosart, 1988: Appalachian cold-air damming. *Mon. Wea. Rev.,* **116,** 137–162.

Buzzi, A., N. Tartaglione, and P. Malguzzi, 1998: Numerical simulations of the 1994 Piedmont flood: Role of orography and moist processes. *Mon. Wea. Rev.,* **126,** 2369–2383.

Chen, W.-D., and R. Smith, 1987: Blocking and deflection of airflow by the Alps. *Mon. Wea. Rev.,* **115,** 2578–2597.

De La Fuente, J., and D. Elder, 1998: The flood of 1997 Klamath National Forest, phase I final report. U.S. Forest Service Tech. Rep., 76 pp.

Doyle, J., 1997: The influence of mesoscale orography on a coastal jet and rainband. *Mon. Wea. Rev.,* **125,** 1465–1488.

Dudhia, J., 1989: Numerical study of convection observed during the winter monsoon experiment using a mesoscale two-dimensional model. *J. Atmos. Sci.,* **46,** 3077–3107.

——, 1993: A nonhydrostatic version of the Penn State–NCAR Mesoscale Model: Validation tests and simulation of an Atlantic cyclone and cold front. *Mon. Wea. Rev.,* **121,** 1493–1513.

Durran, D., and J. Klemp, 1982: On the effects of moisture on the Brunt–Väisälä frequency. *J. Atmos. Sci.,* **39,** 2152–2158.

Ferretti, R., S. Low-Nam, and R. Rotunno, 2000: Numerical simulations of the Piedmont flood of 4–6 November 1994. *Tellus,* **52A,** 162–180.

Groisman, P., and D. Legates, 1994: The accuracy of United States precipitation data. *Bull. Amer. Meteor. Soc.,* **75,** 215–227.

Higgins, R., J.-K. Schemm, W. Shi, and A. Leetma, 2000: Extreme precipitation events in the western United States related to tropical forcing. *J. Climate,* **13,** 793–820.

Hong, S.-Y., and H.-L. Pan, 1996: Nonlocal boundary layer vertical diffusion in a medium-range forecast model. *Mon. Wea. Rev.,* **124,** 2322–2339.

Hunrichs, R., D. Pratt, and R. Meyer, 1998: Magnitude and frequency of the floods of January 1997 in northern and central California—Preliminary determinations. U.S. Geological Survey Open File Rep. 98–626, 120 pp.

Jiang, Q., 2003: Moist dynamics and orographic precipitation. *Tellus,* **55A,** 301–316.

Jones, C., 2000: Occurrence of extreme precipitation events in California and relationships with the Madden–Julian oscillation. *J. Climate,* **13,** 3576–3587.

Kain, J., and J. Fritsch, 1993: Convective parameterization for mesoscale models: The Kain–Fritsch scheme. *The Representation of Cumulus Convection in Numerical Models, Meteor. Monogr.,* No. 46, Amer. Meteor. Soc., 246 pp.

Kalnay, E., and Coauthors, 1996: The NCEP/NCAR 40-Year Reanalysis Project. *Bull. Amer. Meteor. Soc.,* **77,** 437–471.

Lackmann, G., 2002: Cold-frontal potential vorticity maxima, the low-level jet, and moisture transport in extratropical cyclones. *Mon. Wea. Rev.,* **130,** 59–74.

——, and J. Gyakum, 1999: Heavy cold-season precipitation in the northwestern United States: Synoptic climatology and an analysis of the flood of 17–18 January 1986. *Wea. Forecasting,* **14,** 687–700.

Leung, L., Y. Qian, X. Bian, and A. Hunt, 2003: Hydroclimate of the western United States based on observations and regional climate simulation of 1981–2000. Part II: Mesoscale ENSO anomalies. *J. Climate,* **16,** 1912–1928.

Lott, N., D. Ross, and M. Sittel, 1997: The winter of '96–'97 West Coast flooding. National Climatic Data Center, Tech. Rep. 97-01, 22 pp.

Mass, C., D. Ovens, and K. Westrick, 2002: Does increasing horizontal resolution produce more skillful forecasts? *Bull. Amer. Meteor. Soc.,* **83,** 407–430.

Mo, K., and R. Higgins, 1998a: Tropical convection and precipitation regimes in the western United States. *J. Climate,* **11,** 2404–2423.

——, and ——, 1998b: Tropical influences on California precipitation. *J. Climate,* **11,** 412–430.

Ogston, A., D. Cacchione, R. Sternberg, and G. Kineje, 2000: Observations of storm and river flood-driven sediment transport on the northern California continental shelf. *Cont. Shelf Res.,* **20,** 2141–2162.

Overland, J., and N. Bond, 1993: The influence of coastal orography: The Yakutat storm. *Mon. Wea. Rev.,* **121,** 1388–1397.

——, and ——, 1995: Observations and scale analysis of coastal wind jets. *Mon. Wea. Rev.,* **123,** 2934–2941.

Pandey, G., D. Cayan, and K. Georgakakos, 1999: Precipitation structure in the Sierra Nevada of California. *J. Geophys. Res.,* **104** (D10), 12 019–12 030.

Parish, T., 1982: Barrier winds along the Sierra Nevada Mountains. *J. Appl. Meteor.,* **21,** 925–930.

Pierrehumbert, R., 1984: Linear results on the barrier effects of mesoscale mountains. *J. Atmos. Sci.,* **41,** 1356–1367.

——, and B. Wyman, 1985: Upstream effects of mesoscale mountains. *J. Atmos. Sci.,* **42,** 977–1003.

Ralph, F. M., P. J. Neiman, D. E. Kingsmill, P. O. G. Persson, A.

B. White, E. T. Strem, E. D. Andrews, and R. C. Antweiler, 2003: The impact of a prominent rain shadow on flooding in California's Santa Cruz Mountains: A CALJET case study and sensitivity to the ENSO cycle. *J. Hydrometeor.,* **4,** 1243–1264.

Rotunno, R., and R. Ferretti, 2001: Mechanisms of intense Alpine rainfall. *J. Atmos. Sci.,* **58,** 1732–1749.

Smith, R., 1979: The influence of mountains on the atmosphere. *Advances in Geophysics,* Vol. 21, Academic Press, 87–230.

Smolarkiewicz, P., and R. Rotunno, 1989: Low Froude number flow past three-dimensional obstacles. Part I: Baroclinically generated lee vortices. *J. Atmos. Sci.,* **46,** 1154–1164.

——, and ——, 1990: Low Froude number flow past three-dimensional obstacles. Part II: Upwind flow reversal zone. *J. Atmos. Sci.,* **47,** 1498–1511.

Steenburgh, W., and C. Mass, 1996: Interaction of an intense extratropical cyclone with coastal orography. *Mon. Wea. Rev.,* **124,** 1329–1352.

Xiu, Q., 1990: A theoretical study of cold air damming. *J. Atmos. Sci.,* **47,** 2969–2985.